

Study on the mechanism and load characteristics of secondary cavitation near free surface in underwater explosion

Cite as: AIP Advances 12, 105222 (2022); doi: 10.1063/5.0121834

Submitted: 19 August 2022 • Accepted: 27 September 2022 •

Published Online: 28 October 2022




View Online



Export Citation



CrossMark

Jun Yu (余俊),^{1,2,a)}  Wen-Wei Wu (吴文伟),^{1,2} Bo Yan (严波),¹ Jiu-Ting Dong (董玖亭),¹ and Xian-Pi Zhang (张显丕)¹

AFFILIATIONS

¹China Ship Scientific Research Center, Wuxi 214082, China

²Taihu Laboratory of Deep-sea Technological Science, Wuxi 214082, China

^{a)}Author to whom correspondence should be addressed: yujun@cssrc.com.cn

ABSTRACT

Although the cavitation phenomenon in underwater explosion has been researched for more than 100 years, the phase transition models based on mass and heat exchange between liquid and its vapor phases have only been established in the past decade. In this study, the secondary cavitation phenomenon was first captured by phase transition based on a four-equation system. The bulk cavitation near the free surface induced by underwater explosion was numerically investigated, and three typical bulk cavitation cases were investigated to explore their motion mechanisms and load characteristics on hydrodynamics and phase transition generation. It was found that secondary bulk cavitation will occur only under the condition that both the initial shock wave intensity and the distance between the water surface and the explosion bubble are satisfied in a specific relationship. Producing bulk cavitation was difficult at a relatively deep detonation depth because of the weak rarefaction wave reflected from the water surface by smaller charges. The statistical data under the condition of small charge indicated that the duration of cavitation increases with the increase in charge weight but the growth trend slows down gradually. However, the maximum volume of cavitation increased linearly with an increase in the charge weight. The present results can expand the currently limited database of underwater explosion multiphase fluids and provide insight into the interactions between the shock wave, bulk cavitation, explosion bubble, and water surface.

© 2022 Author(s). All article content, except where otherwise noted, is licensed under a Creative Commons Attribution (CC BY) license (<http://creativecommons.org/licenses/by/4.0/>). <https://doi.org/10.1063/5.0121834>

I. INTRODUCTION

Underwater explosion (UNDEX) has attracted considerable attention for more than 100 years because of its great military and civilian value.¹⁻⁴ The underwater explosion phenomenon can be classified into three main stages: explosive detonation, shock wave propagation, and bubble movement. The high-temperature and high-pressure gas produced by underwater explosives propagates strong shock waves in the surrounding water and the explosion bubble expands outward simultaneously. When the shock wave reaches the water surface or structure interface, the water surface or structure movement can lead to rarefaction wave appearance, which can easily induce bulk cavitation or local cavitation phenomena.

Bulk cavitation induced by underwater explosion near the free surface has been observed since 1919.⁵ Underwater explosion bubble clouds can be tens of meters deep and hundreds of meters in diameter and block sound transmission and induce additional load on nearby structures.^{6,7} Kennard first predicted the size of bulk cavitation based on the size and depth of explosives.^{8,9} The detonation shock wave is simplified as a shock with an exponential tail whose properties depend on the charge's depth and weight.^{10,11} This method of imaging is first used to simulate the reflection off the water surface by placing a virtual source above the water surface with a magnitude equal to that of the real explosive source with an opposite phase. Therefore, the absolute pressure is the sum of the pressures owing to the real source, virtual source, and ambient (environment) pressure. This means that whenever the absolute

pressure falls below the saturated pressure, the water will cavitate, which has become the theoretical basis of most modern cavitation models. This theory was used to simulate the bulk cavitation detonated at a 5 cm depth for a 5 g 2,4,6-trinitrotoluene (TNT) charge, and the direct, reflected, and ambient pressures were all present.¹¹ Another model was built to set the absolute pressure equal to 0 Pa at the top cavitation cloud boundary, and the decay rates of the incident and reflected pressures at the bottom boundary are equal to each other.^{12–14}

In the experiment study of bulk cavitation, 30.8 kg pentolite (PENT) charge exploded beneath water, and the absolute pressure was measured,¹⁵ which has been used by several researchers to verify the numerical model of cavitation.^{16,17} The schlieren-type images of the cavitation were investigated experimentally, and some structural features within the bulk cavitation in underwater explosion were revealed.¹⁸ Extensive cavitation phenomena have been observed by high-speed video images in small-scale experiments of simple target cylinders or near the water surface.^{19,20}

Although much research has been conducted on the theoretical model and experimental data of cavitation, it is difficult to understand the evolution mechanism of cavitation owing to the limitations of basic assumptions, experimental data types, and other factors. On the other hand, numerical simulations have attracted great attention in the past two decades owing to the detailed information provided by some cavitation models, and many cavitation models have been proposed. The earliest cavitation model used extensively in UNDEX can be reduced to the cut-off model.²¹ In this model, the pressure is equal to the given value when the fluid pressure is lower than the constant pressure. An isentropic one-fluid model was built to treat the fluid as a homogeneous mixture comprising isentropic vapor and liquid phases.²² The Schmidt model was used to efficiently simulate the cavitation flow occurring in high-pressure and high-velocity nozzles.²³ A modified Schmidt model was proposed to improve the application of the Schmidt model in unsteady transient cavitation flows.²⁴ A new isentropic cavitation model was adopted to simulate underwater explosion cavitation, based on a reduced five-equation system.²⁵ These models can be classified as one-fluid cavitation models, which cannot predict the mechanism of mass and heat conversion between the liquid and its vapor phases in the cavitation region. However, several two-fluid cavitation models have been established over the past decade to understand the mechanism of the vapor–liquid phase transition in cavitation. The seven-equation was first proposed to simulate the mass exchange between two-phase mixtures in detonation simulation,²⁶ which provided a basic model for the two-fluid cavitation model and showed great capability in describing complex wave patterns and thermodynamic dynamics in cavitation. Pelanti and Shyue^{27,28} developed a new multiphase flow computational model based on a six-equation system that can efficiently deal with cavitation and evaporation waves. A phase transition model based on a four-equation system was proposed to compute the thermodynamic equilibrium between the liquid and its vapor phases, which had been expanded to multicomponent fluid motion with phase transition.^{29,30} This model was used to investigate cavitation evolution in underwater explosion, and the fine characteristics of the flow field in the cavitation domain can be captured.^{31,32} Another phase transition model based on a five-equation system using temperature and chemical relaxation

with the monotonic mixture speed of sound was developed by Zhang.³³

Given the complexity of multiphase flow in cavitation motion and its importance in warship damage analysis in underwater explosion, it is necessary to explore the motion and load characteristics of cavitation. Without loss of generality, in this study, we investigated the cavitation behavior induced by multi-weight charges exploded at different depths in the two-dimensional axisymmetric domain. The cavitation near the free surface was numerically studied using the phase transition model based on a four-equation system. The remainder of this paper is organized as follows: the description of the numerical method is presented in Sec. II. Numerical studies on the cavitation near free surface are presented in Sec. III to identify the cavitation domain and pressure contour plots, cavitation volume evolution, and secondary cavitation phenomena. Finally, Sec. IV concludes the paper.

II. NUMERICAL METHOD

Underwater explosion involves the generation and propagation of strong shock waves, and its dynamics are governed by multiphase compressible fluid equations. The two-dimensional compressible Euler equation can be expressed as^{30,32}

$$\frac{\partial Q}{\partial t} + \frac{\partial F}{\partial x} + \frac{\partial G}{\partial y} = S,$$

where $Q = [\rho, \rho u, \rho v, \rho E]^T$, $F = [\rho u, \rho u^2 + p, \rho uv, (\rho E + p)u]^T$, $G = [\rho v, \rho uv, \rho v^2 + p, (\rho E + p)v]^T$. S is the source term related to body force; ρ is the fluid density; u and v are velocity components of the x and y axis, respectively; p is the pressure; and E is the total energy per unit mass. Both the viscosity and thermal effects in the fluid are ignored.

In the multiphase fluid model, it can be assumed that each component of the mixture occupies its own separate volume. Under this assumption, all mass balance equations can be written as^{30,32}

$$\frac{\partial \rho Y_k}{\partial t} + \text{div}(\rho Y_k \mathbf{u}) = 0,$$

where subscript k refers to various physical and chemical components and \mathbf{u} is the velocity vector. Therefore, Y_k is the mass fraction of the k -th species in the entire mixture fluid. It can be observed that the conservation equation for each species within the mixture has the same formula as the total mass conservation equation Eq. (1). Without loss of generality, parameter k can be specified as follows: $k = 1$ for the liquid phase, $k = 2$ for its vapor phase, and $k = 3, \dots, N$ for other non-condensable gases.

During the phase transition process, the mixture specific volume $v = 1/\rho$ and the internal energy e do not vary under the assumption of constant pressure and velocity. The mass fractions of the liquid and its vapor phases remain constant. Although the pressure and temperature vary and reach their equilibrium values (p^* , T^*), the phase transition model will change to compute the equilibrium state (p^* , T^* , $Y_{k=1,2}$) from state (v , e , p , T , Y_k).

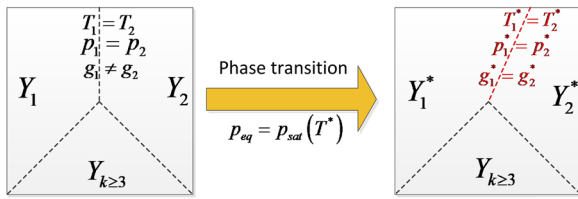


FIG. 1. Schematic diagram of mass fraction distribution of different phases in fluid before and after phase transition treatment. The dotted lines represent the location of the volume division boundary.³²

Therefore, under the assumption of mechanical and thermal equilibrium, the mixture fluid satisfies^{30,33}

$$\begin{cases} T = T_k, p = p_k, \forall k, \\ v = \sum_{k=1}^N Y_k v_k; e = \sum_{k=1}^N Y_k e_k. \end{cases}$$

This system contains four unknown variables with four equations, which can be solved using Newton’s iterative method.³⁰ Therefore, the phase transition model ensures that the final equilibrium state (p^*, T^*) is saturated at each step, as shown in Fig. 1.³²

The computational domain is shown in Fig. 2. A two-dimensional (2D) axisymmetric model was used to simulate the

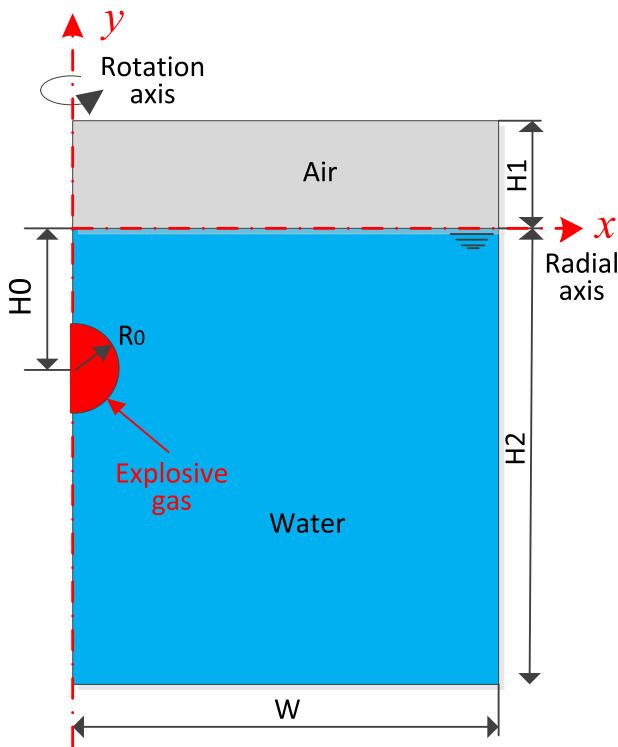


FIG. 2. Schematic of underwater explosion near the free surface.

movement of the multiphase fluids. The initial flow field of the computational domain consisted of three main regions: the explosion gas, water, and air. A symmetrical boundary condition was imposed on the y -axis, and non-reflection characteristic boundary conditions were applied to the other boundaries. The numerical method of the multiphase compressible fluid model in the present study was previously validated by various cases involving phase transition evolution.^{31,32}

III. RESULTS AND DISCUSSIONS

A. Cavitation near the free surface in small-charge underwater explosion

In this section, we first consider the cavitation near the free surface generated by a small-charge underwater explosion. Five underwater explosion cases were simulated to explode at 0.5 m water depth, as summarized in Table I. The parameters in the table can refer to Fig. 2. The initial radius of the charge was R_0 , and the distance from the center of the sphere charge to the water surface was H_0 , where H_1 and H_2 are the thicknesses of the air and water domains, respectively. The radial length of the computational domain was W . The parameter dx is the spatial step of the uniform grid in the x -axis, and $dy = dx$, which means that the computational domain is divided by uniform meshes.

Figure 3 shows the cavitation domain and pressure contour plots at times of 0.42, 0.69, 0.83, and 0.97 ms under a 5 g TNT charge case exploded at 0.5 m water depth. In the cavitation domain contour plots, the red area indicates the cavitation domain in the upper contour plots, and the other colored areas denote the water, air, and explosion bubble domains. The cavitation domain appeared after which the explosion shock wave is reflected into the rarefaction wave from the water surface at the initial time (0.41 ms). As the rarefaction wave continues to propagate, the cavitation domain increases continuously at 0.74 ms. Subsequently, as the high-pressure region below the cavitation domain propagates upward, the cavitation domain gradually decreased and eventually disappears (as shown at 0.99 and 1.21 ms). Figures 4 and 5 show the cavitation domain and pressure contour plots at typical times under the 200 and 1000 g TNT charge cases at 0.5 m water depth, respectively. It can be observed that the maximum volume and duration of the cavitation domain increase with an increase in the charge weight.

Figure 6 shows the time-history curve of the evolution of the cavitation domain volume and the statistics of the duration (period) and maximum volume of the cavitation domain under different

TABLE I. Simulation cases for the charge exploded at 0.5 m water depth.

TNT charge (g)	R_0 (m)	H_0 (m)	H_1 (m)	H_2 (m)	W (m)	dx (m)
5	0.009					0.001
50	0.020					0.002
200	0.031	0.5	1	5	4	0.003
500	0.042					0.004
1000	0.053					0.005

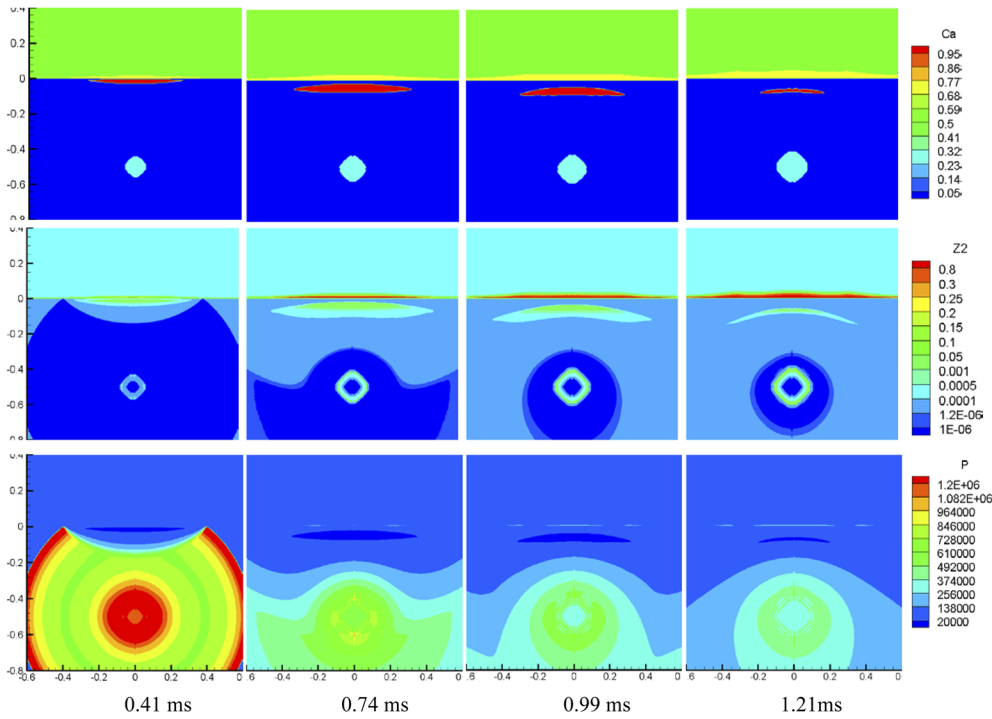


FIG. 3. Numerical results of the cavitation domain, vapor volume fraction, and pressure contour plot (from up to down) at different times $t = 0.42, 0.69, 0.83,$ and 0.97 ms (from left to right) under 5 g TNT charge explosion at 0.5 m water depth. The red area indicates the cavitation domain in the upper contour plots, and other areas denote water, air, and explosion bubble domains.

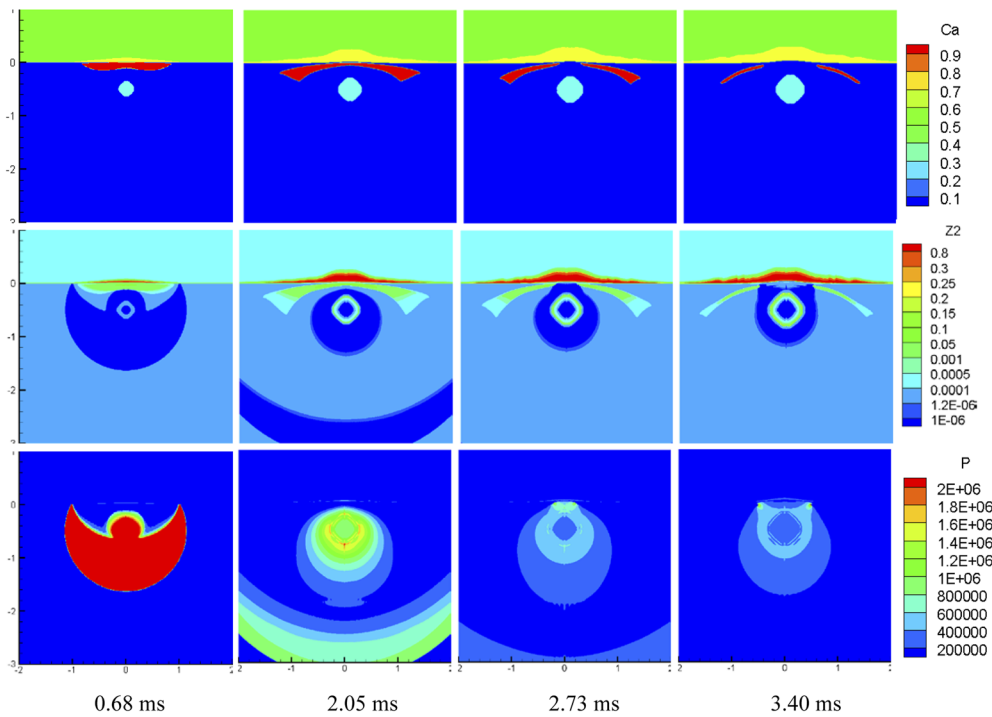


FIG. 4. Numerical results of the cavitation domain, vapor volume fraction, and pressure contour plot (from up to down) at different times $t = 0.68, 2.05, 2.73,$ and 3.40 ms (from left to right) under 200 g TNT charge explosion at 0.5 m water depth. The red area indicates the cavitation domain in the upper contour plots, and other areas denote water, air, and explosion bubble domains.

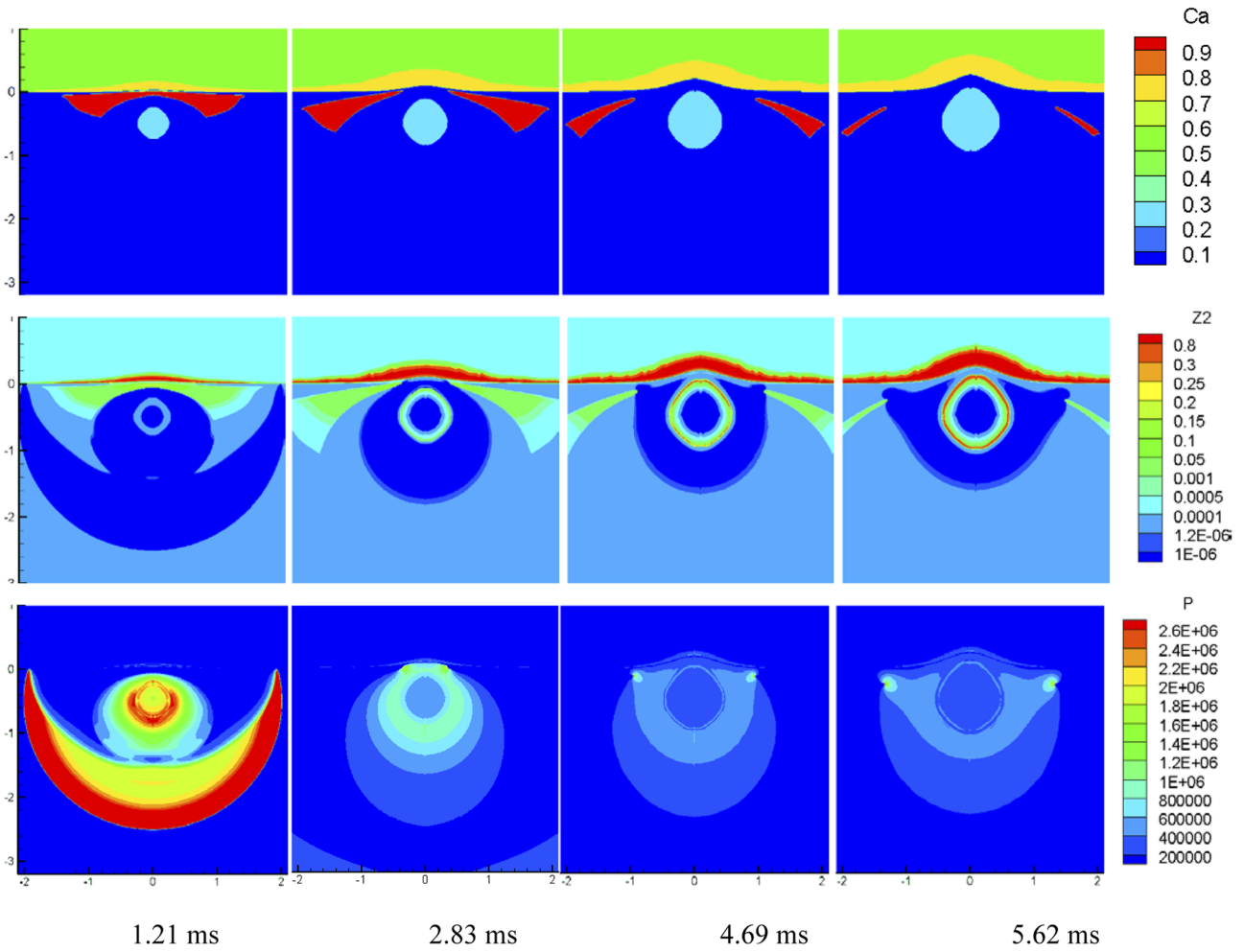


FIG. 5. Numerical results of the cavitation domain, vapor volume fraction, and pressure contour plot (from up to down) at different times $t = 1.21, 2.83, 4.69,$ and 5.62 ms (from left to right) under 1000 g TNT charge explosion at 0.5 m water depth. The red area indicates the cavitation domain in the upper contour plots, and other areas denote water, air, and explosion bubble domains.

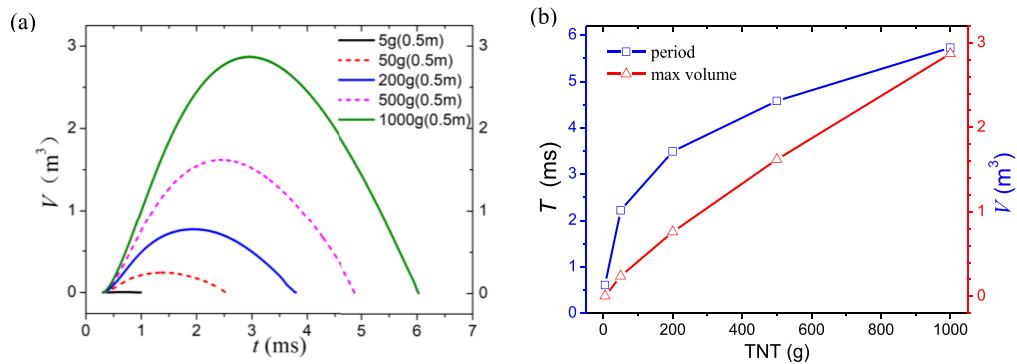


FIG. 6. (a) Time-history curve of the evolution of the cavitation domain volume and (b) the statistics of the duration (period) and maximum volume at 0.5 m water depth.

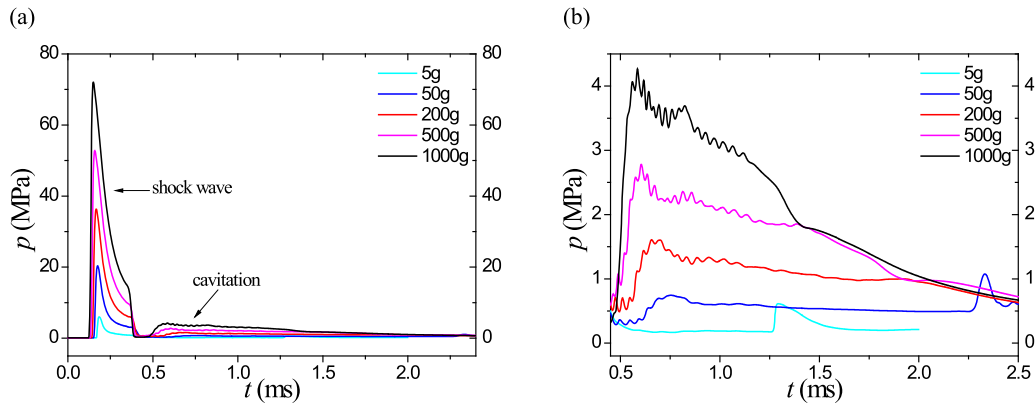


FIG. 7. Pressure–time-history curves for the location of (0, -0.2) m under multi-charge explosion at 0.5 m water depth. (a) Pressure in the whole stage. (b) Pressure in the cavitation stage.

weight explosives. As shown in Fig. 6(a), the expansion time of the cavitation domain is essentially the same as that of the contraction stage, which is very similar to the motion law of the explosion bubble underwater. The biggest difference between the two is that when the cavitation domain shrinks, the overall shape is flat, where the explosion bubble is generally spherical or jet shaped. The curve of the 5 g charge case shown in Fig. 6 is close to a straight line because the cavitation volume is too small compared with other cases

(the maximum volume is $\sim 0.004 \text{ m}^3$). Figure 6(b) shows that the duration of cavitation increases with an increase in the charge weight but the growth trend slows down gradually. However, the maximum volume of cavitation increased linearly with an increase in the charge weight. A comparison of the time history of the pressure at coordinates (0, -0.2) is shown in Fig. 7(a). It can be observed that the pressure produced by the cavitation occurred immediately after the shock wave pressure. Figure 7(b) shows the details of the

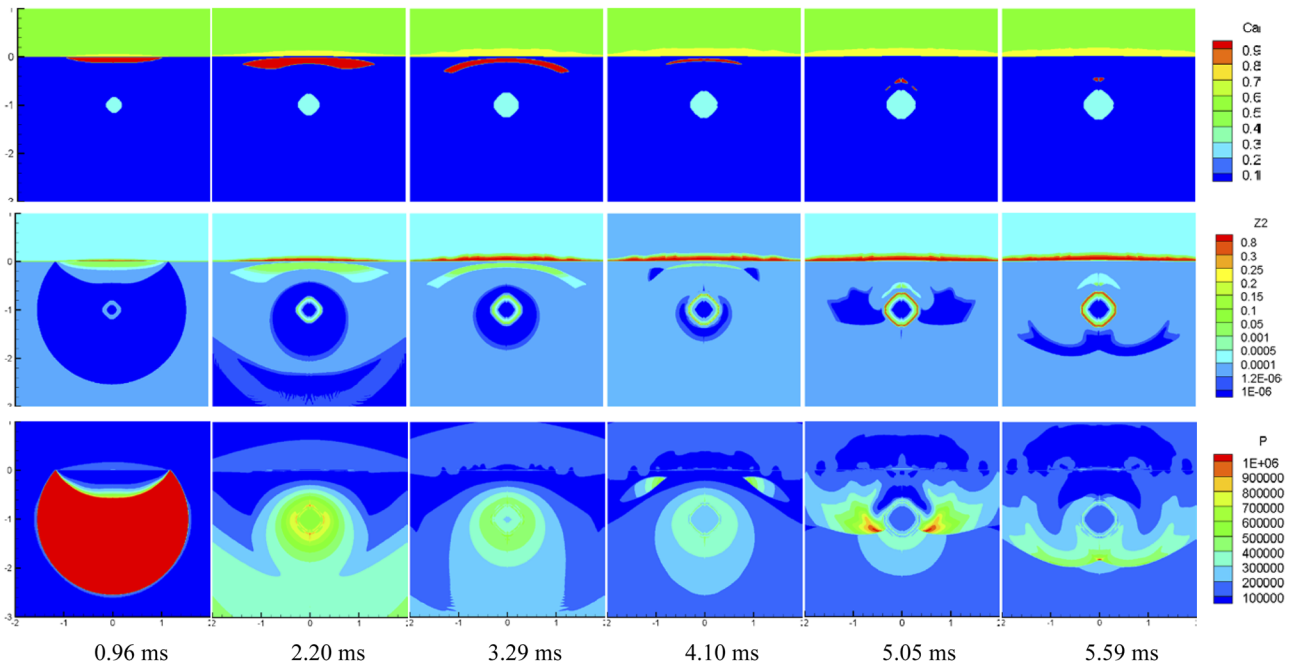


FIG. 8. Numerical results of the cavitation domain, vapor volume fraction, and pressure contour plot (from up to down) at different times $t = 0.96, 2.20, 3.29, 4.10, 5.05,$ and 5.59 ms (from left to right) under 200 g TNT charge explosion at 1.0 m water depth. The red area indicates the cavitation domain in the upper contour plots, and other areas denote water, air, and explosion bubble domains.

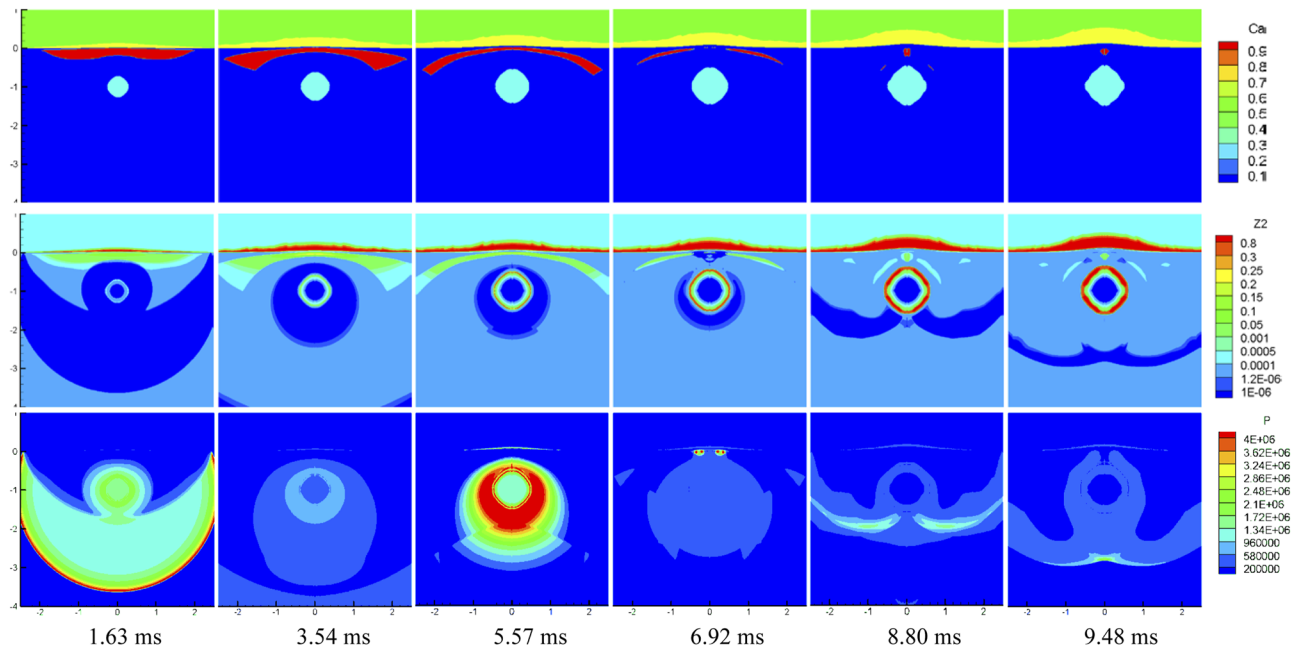


FIG. 9. Numerical results of the cavitation domain, vapor volume fraction, and pressure contour plot (from up to down) at different times $t = 1.63, 3.54, 5.57, 6.92, 8.80,$ and 9.48 ms (from left to right) under 1000 g TNT charge explosion at 1.0 m water depth. The red area indicates the cavitation domain in the upper contour plots, and other areas denote water, air, and explosion bubble domains.

cavitation pressure for different cases. It was found that the maximum cavitation pressure increased with an increase in the charge weight. Although the peak cavitation pressure was lower than that of the shock wave, it remained longer.

B. Secondary cavitation near the free surface in small-charge underwater explosion

We only observed cavitation once in the aforementioned underwater explosion cases. It is known that the generation of cavitation is closely related to the intensity and duration of rarefaction

waves reflected by the free surface and the rarefaction wave is related to the distance from the free surface to the charge. Therefore, the initial depth of the explosive plays an important role in the cavitation behavior. In this section, the explosion depth was changed to 1 m, and the others remained unchanged, as listed in Table I. In this new condition, the case of a 5 g TNT charge has no obvious cavitation domain. This is due to the fact that the rarefaction wave reflected from the shock wave on the free surface is weak in the case and the volume fraction of vapor phase in the water near the free surface is lower than the critical threshold of cavitation occurrence. For the case of a 50 g TNT charge, the cavitation domain can be

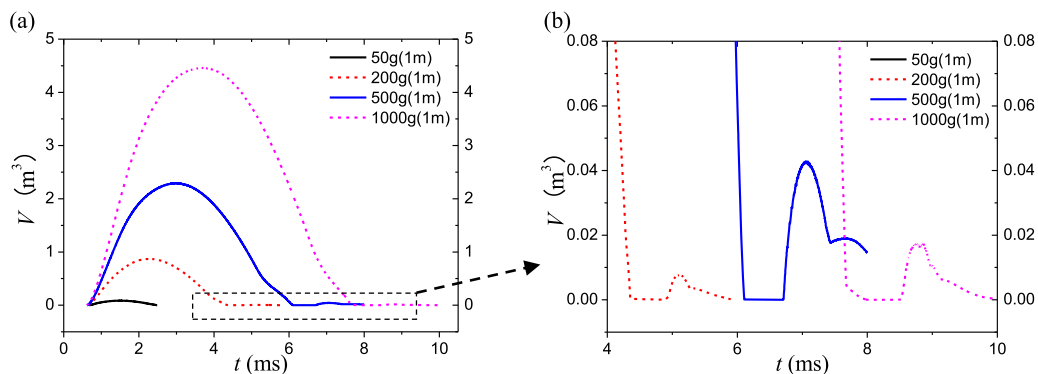


FIG. 10. Time-history curve of cavitation domain volume when different charges explode at 1 m water depth. (a) The whole stage. (b) The secondary cavitation stage.

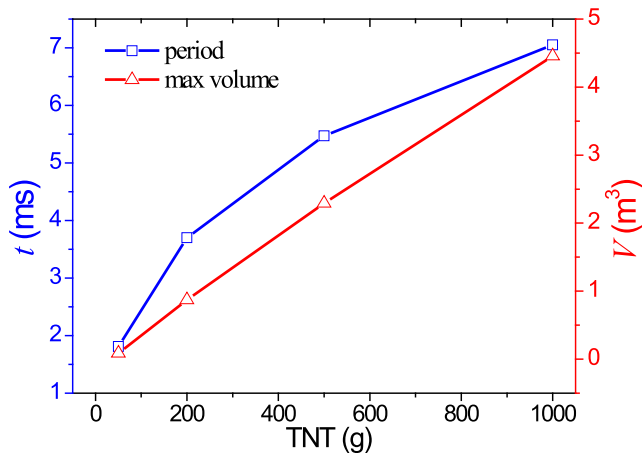


FIG. 11. Statistics of the duration (period) and maximum volume of the cavitation domain under small-charge exploded at 1 m water depth.

observed. The evolution of the cavitation is similar to that in the aforementioned cases.

Figure 8 shows the cavitation domain and pressure contour plots for the 200 g TNT charge explosion case exploded at a water depth of 1 m. It can be observed that the secondary cavitation occurred after the first cavitation collapse at about 5.05 ms. It is found from the pressure contour plot that the low-pressure region is distributed around the explosion bubble and gradually moves upward. Therefore, it is reasonable to assume that the second cavitation was caused by the reflection of the rarefaction wave from the interface of the explosion bubble. Two cavitation phenomena can also be observed for 500 and 1000 g of TNT charges. Figure 9 shows the cavitation domain and pressure contour plots for the 1000 g TNT charge explosion case exploded at a water depth of 1 m.

Figure 10(a) shows the time-history curve of the cavitation domain volume evolution and the statistics of the duration (period) and maximum volume of the cavitation domain for different weight explosives. The secondary cavitation curve is shown in Fig. 10(b).

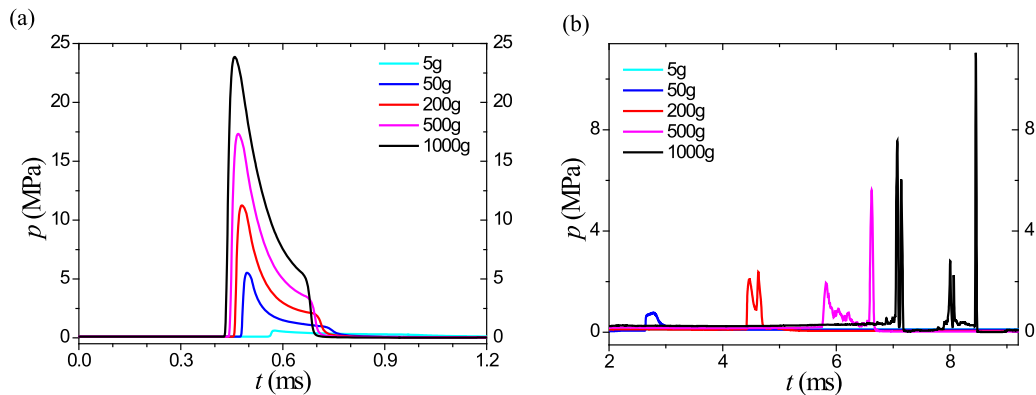


FIG. 12. Pressure–time-history curves for the location of (0, -0.2) m under multi-charge explosion at 0.5 m water depth. (a) Pressure in the shock wave stage. (b) Pressure in the cavitation stage.

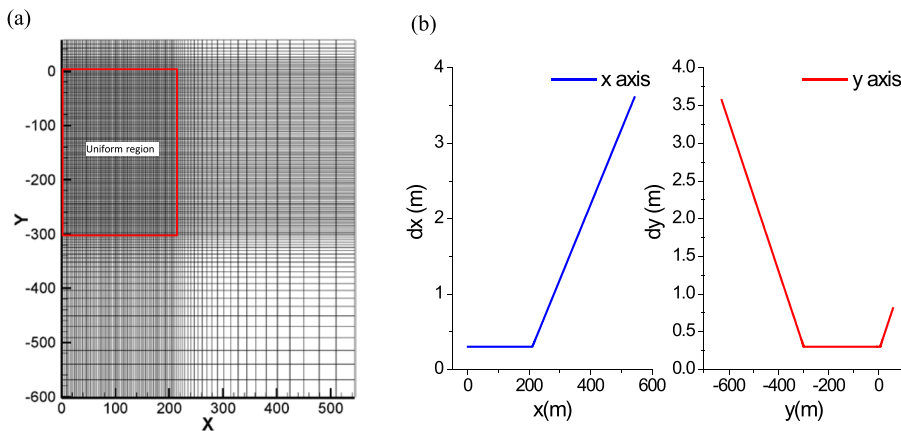


FIG. 13. Mesh strategy of the fluid domain; every one in ten of the lines is plotted on the left figure.

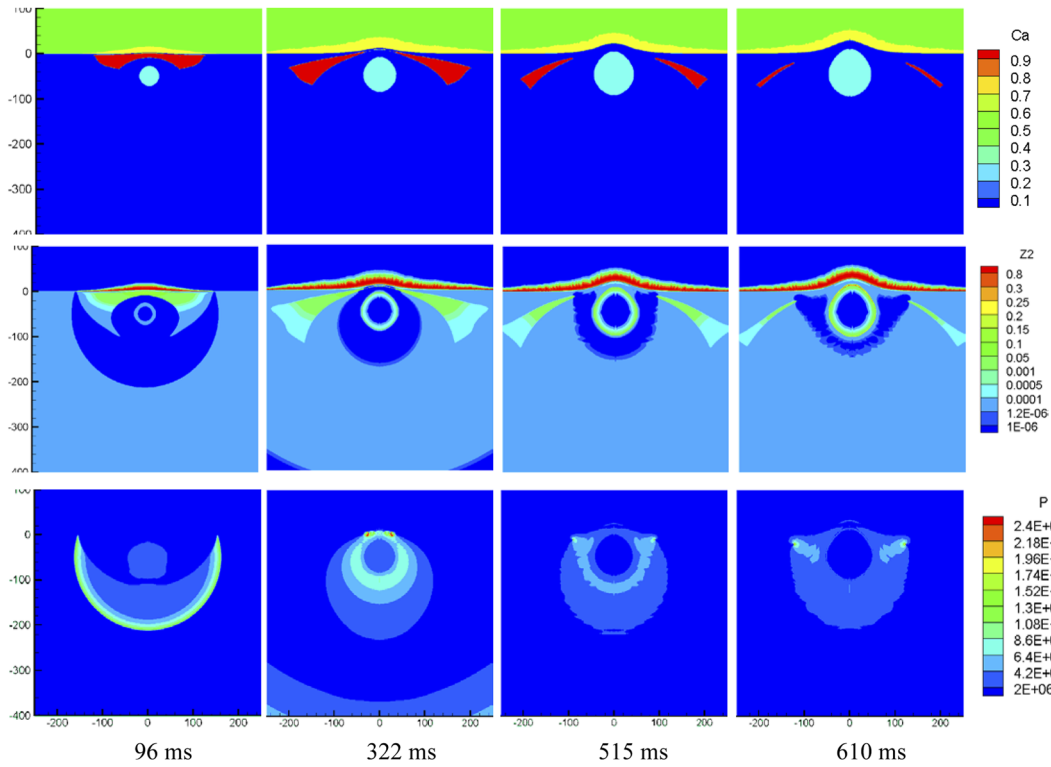


FIG. 14. Numerical results of the cavitation domain, vapor volume fraction, and pressure contour plot (from up to down) at different times $t = 96, 322, 515,$ and 610 ms (from left to right) under 1000 tons of TNT charge explosion at 50 m water depth. The red area indicates the cavitation domain in the upper contour plots, and other areas denote water, air, and explosion bubble domain.

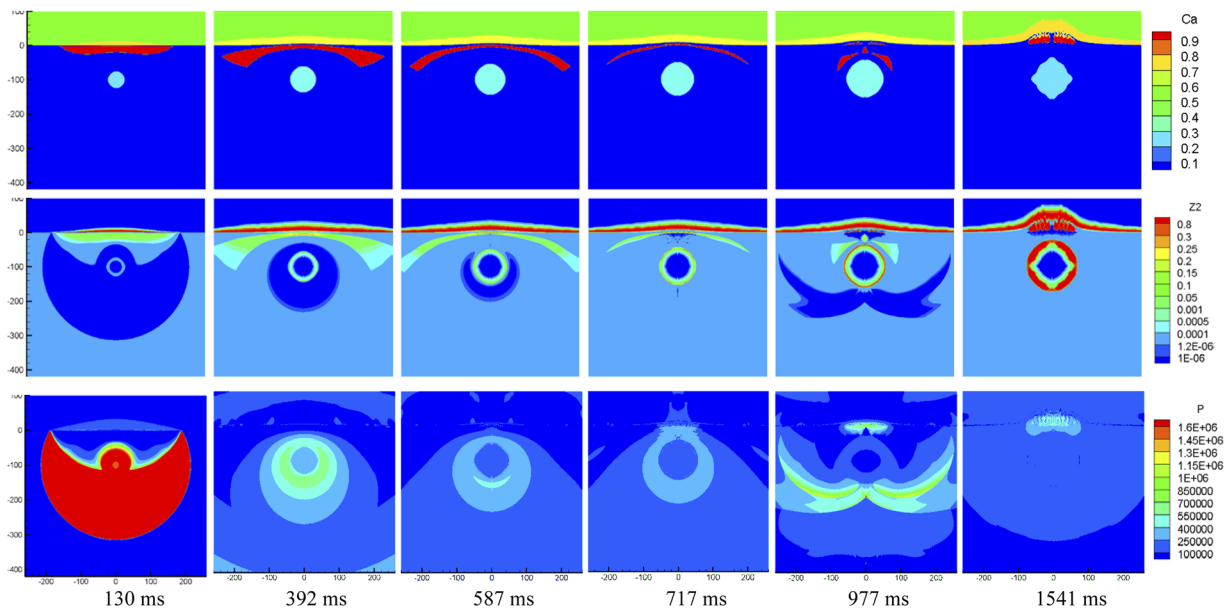


FIG. 15. Numerical results of the cavitation domain, vapor volume fraction, and pressure contour plot (from up to down) at different times $t = 130, 392, 587, 717, 977,$ and 1541 ms (from left to right) under 1000 tons of TNT charge explosion at 100 m water depth. The red area indicates the cavitation domain in the upper contour plots, and other areas denote water, air, and explosion bubble domain.

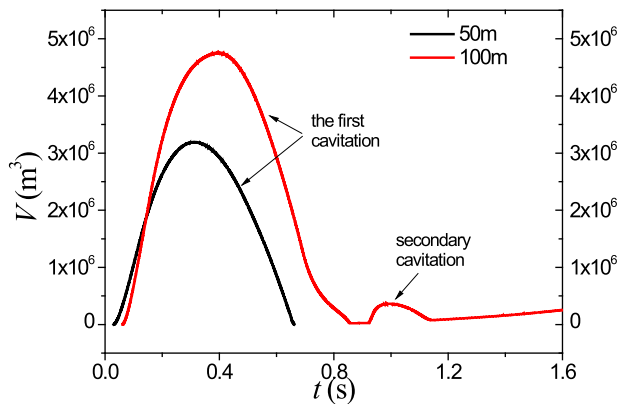


FIG. 16. Time-history curve of cavitation domain volume when 1000 tons of TNT charge exploded at 50 and 100 m water depth.

Figure 11 shows that the duration of cavitation increases with an increase in the charge weight but the growth trend slows gradually. However, the maximum volume of cavitation increased linearly with an increase in the charge weight. These conclusions are similar to those shown in Fig. 6(b).

A comparison of the time history of the pressure at coordinates (0, -0.2) is shown in Fig. 12. It can be observed that although the pressure in the shock wave stage is obviously less than that in the same charge cases at the 0.5 m detonation depth, the cavitation pressure is greater than the same charge cases at the 0.5 m detonation depth.

C. Cavitation near the free surface in super big charge underwater explosion

It can be seen from the above-mentioned cases that both the detonation depth and charge weight have an important influence on cavitation near the free surface in underwater explosion. An important manifestation of cavitation in underwater explosion is underwater nuclear explosion. To some extent, nuclear explosion

can be simplified to the explosion phenomenon of giant underwater explosives. The cavitation phenomenon induced by giant underwater explosives can be approximately simulated using the phase transition model.

In this section, the cavitation caused by 1000 tons of TNT explosives detonated at 50 and 100 m water depths was simulated. A non-uniform mesh was adopted for the spatial discretization of the entire domain, as shown in Fig. 13(a). The computational domain contains a uniform zone around the explosive, where the other areas are non-uniform grids. Figure 13(b) shows the distribution of the spatial steps in the x and y directions. The radius of the spherical explosive is ~ 5.3 m, and the computational domain was $(0, 540) \times (-600, 60)$ m².

Figure 14 displays the cavitation domain and pressure contour plots at different times under 1000 tons of TNT charge explosion at a water depth of 50 m. No secondary cavitation is observed in the numerical results. This can be attributed to the small distance between the water surface and the explosion bubble at 610 ms in the first cavitation collapse stage, as shown in Fig. 14. Figure 15 shows the numerical results at 100 m water depth. The numerical results clearly display that secondary cavitation appears soon after the first cavitation collapse. It can also be observed that the partial cavitation domain is distributed around the explosion bubble at the initial stage of the formation of the secondary cavitation at 977 ms. The biggest difference is that the regional shape of the secondary cavitation in the large-charge case is very complex. The cavitation domain looks like a bunch of flames.

Figure 16 illustrates the time-history curve of the cavitation domain volume evolution under different detonation depths. It can be found that there are two distinct stages of cavitation. The maximum volume of the secondary cavitation was $\sim 1/13$ of that of the first cavitation. A comparison of the time-history of the pressure at coordinates (0, -5) m is shown in Fig. 17. It can be observed that although the peak pressure in the shock wave stage is high, the loading time is only 7 ms. However, the loading time of cavitation for the two cases is more than 1.0 s, which cannot be ignored for its impact damage effect on underwater low frequency structures.

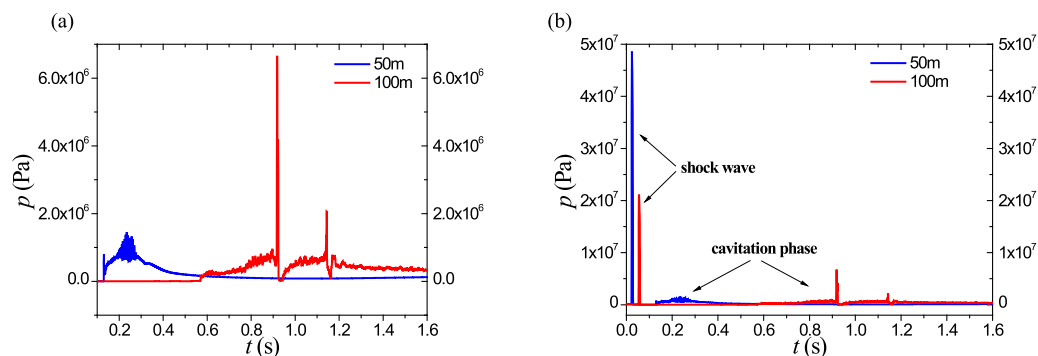


FIG. 17. Pressure-time-history curves for the location of (0, -5) m when 1000 tons of TNT charge exploded at 50 and 100 m water depth. (a) Pressure curve of the shock wave stage. (b) Pressure curve of the cavitation stage.

IV. CONCLUSIONS

In this study, bulk cavitation near a free surface induced by underwater explosion was numerically studied using a phase transition model based on a four-equation system. Three typical bulk cavitation cases were investigated to explore their motion mechanisms and load characteristics on hydrodynamics and phase transition generation.

The first example is the cavitation caused by a variety of small charges at shallow detonation depths. The results show that the occurrence of the creation, development, and collapse of bulk cavitation can be accurately captured by the phase transition model. The second example is the cavitation induced by the same series of small charges at a relatively deep detonation depth. It is found that the bulk cavitation is difficult to produce due to weak rarefaction waves reflected from the water surface by the minimum charge. Specifically, the secondary cavitation phenomenon was captured in the case of relatively large charges. These secondary cavitations began to appear mainly around the explosion bubble and then gradually moved upward until they disappeared. The third example is the cavitation induced by a large charge, which can be used to evaluate the bulk cavitation effect under the condition of an underwater nuclear explosion. Although the charge weight is sufficiently large, secondary cavitation does not occur at shallow detonation depth. This can be attributed to the small distance between the water surface and the upper wall of the explosion bubble when the first cavitation disappears, which prevents the generation of secondary cavitation. In the case of a relatively deep detonation depth, secondary bulk cavitation occurs because the initial shock wave intensity and the distance between the water surface and the explosion bubble are satisfied. The secondary bulk cavitation induced in this special environment is similar to a burning flame.

The present results can expand the currently limited database of multiphase fluid in underwater explosion and also provide insight into the interaction between the shock wave, bulk cavitation, explosion bubble, and water surface. The experimental study of underwater explosion cavitation is also a very important work, and we are working out a corresponding research plan to further verify the numerical simulation results.

AUTHOR DECLARATIONS

Conflict of Interest

The authors have no conflicts to disclose.

Author Contributions

Jun Yu: Conceptualization (equal); Methodology (equal); Writing – original draft (equal). **Wen-Wei Wu:** Formal analysis (equal); Resources (equal); Supervision (equal). **Bo Yan:** Data curation (equal); Software (equal); Validation (equal); Visualization (equal). **Jiu-Ting Dong:** Methodology (equal); Software (equal); Visualization (equal). **Xian-Pi Zhang:** Data curation (equal); Investigation (equal); Resources (equal).

DATA AVAILABILITY

The data that support the findings of this study are available from the corresponding author upon reasonable request.

REFERENCES

- R. H. Cole, *Underwater Explosion* (Princeton University Press, NJ, 1948), pp. 3–8.
- J. H. Liu, “Theory and its applications of ship dynamic responses to non-contact underwater explosions,” Ph.D. thesis, CSSRC, Wuxi, China, 2002, pp. 5–8.
- J. J. Esplin, “Bulk cavitation extent modeling: An energy-based approach,” Ph.D. thesis (The Pennsylvania State University, 2016), pp. 1–8.
- J. Yu, G.-z. Liu, J. Wang, and H.-k. Wang, “An effective method for modeling the load of bubble jet in underwater explosion near the wall,” *Ocean Eng.* **220**, 108408 (2021).
- H. Hilliar, “Experiments on the pressure wave thrown out by submarine explosions,” *Underwater Explos. Res.* **1**, 65–189 (1919).
- S. H. Ahn, “Investigation of shallow UNDEX in littoral ocean domain,” Ph.D. thesis (Naval Postgraduate School, Monterey, CA, 2014), pp. 15–20.
- J. M. Didoszak, “Parametric studies of DDG-81 ship shock trial simulations,” Ph.D. thesis (Naval Postgraduate School, Monterey, CA, 2004), pp. 5–7.
- E. H. Kennard, “Explosive load on underwater structures as modified by bulk cavitation,” Technical Report No. DTMB-511, David Taylor Model Basin, Washington, DC, 1943.
- E. H. Kennard, “Cavitation in an elastic liquid,” *Phys. Rev.* **63**, 172–181 (1943).
- J. F. Slifko, “Pressure-pulse characteristics of deep explosions as functions of depth and range,” Technical Report No. NOLTR-67-87, Naval Ordnance Laboratory, White Oak, MD, 1967.
- N. R. Chapman, “Measurement of the waveform parameters of shallow explosive charges,” *J. Acoust. Soc. Am.* **78**(2), 672–681 (1985).
- A. Arons, D. Yennie, and T. Cotter, “Long range shock propagation in underwater explosion phenomena II,” *Underwater Explos. Compend.* **1**, 107 (1949).
- F. A. Costanzo and J. D. Gordon, “A solution to the axisymmetric bulk cavitation problem,” in *53rd Shock and Vibration Bulletin* (Shock and Vibration Information Center, Naval Research Laboratory, Washington, DC, 1983).
- A. P. Walters, “Investigation of an explicitly modeled solid ocean floor on a shallow water UNDEX event,” Ph.D. thesis, Naval Postgraduate School, Monterey, CA, 2011.
- M. H. Marcus, “The response of a cylindrical shell to bulk cavitation loading,” Report No. NSWCTR 81-295, 1983.
- Z. Zong, G. Chen, F. Ye, H. T. Li, and Y. J. Zhao, “Numerical simulation of cavitation caused by underwater explosion,” *J. Ship Mech.* **18**, 385–394 (2014).
- W. Wu, Y.-L. Liu, A.-M. Zhang, N. Liu, and L. Liu, “Numerical investigation on underwater explosion cavitation characteristics near water wave,” *Ocean Eng.* **205**, 107321 (2020).
- H. Kleine, S. Tepper, K. Takehara, T. G. Etoh, and K. Hiraki, “Cavitation induced by low-speed underwater impact,” *Int. J. Shock Waves* **19**, 895 (2009).
- J. M. Brett and G. Yiannakopoulos, “A study of explosive effects in close to proximity to a submerged cylinder,” *Int. J. Impact Eng.* **35**, 206–225 (2008).
- P. Cui, A. M. Zhang, and S. P. Wang, “Small-charge underwater explosion bubble experiments under various boundary conditions,” *Phys. Fluids* **28**, 117103 (2016).
- J. E. Van Aanhold, G. J. Meijer, and P. P. M. Lemmen, “Underwater shock response analysis on a floating vessel,” *Shock Vib.* **5**, 53–59 (1998).
- T. G. Liu, B. C. Khoo, and W. F. Xie, “Isentropic one-fluid modelling of unsteady cavitating flow,” *J. Comput. Phys.* **201**, 80–108 (2004).
- D. P. Schmidt, C. J. Rutland, and M. L. Corradini, “A fully compressible, two-dimensional model of small, high speed, cavitating nozzles,” *Atomization Sprays* **9**, 255–276 (1999).

- ²⁴W. F. Xie, T. G. Liu, and B. C. Khoo, "Application of a one-fluid model for large scale homogeneous unsteady cavitation: The modified Schmidt model," *Comput. Fluids* **35**, 1177–1192 (2006).
- ²⁵A. Daramizadeh and M. R. Ansari, "Numerical simulation of underwater explosion near air–water free surface using a five-equation reduced model," *Ocean Eng.* **110**, 25–35 (2015).
- ²⁶M. R. Baer and J. W. Nunziato, "A two-phase mixture theory for the deflagration-to-detonation transition (DDT) in reactive granular materials," *Int. J. Multiphase Flow* **12**(6), 861 (1986).
- ²⁷M. Pelanti and K.-M. Shyue, "A mixture-energy-consistent six-equation two-phase numerical model for fluid with interfaces, cavitation and evaporation waves," *J. Comput. Phys.* **259**, 331–357 (2014).
- ²⁸M. Pelanti and K.-M. Shyue, "A numerical model for multiphase liquid–vapor–gas flows with interfaces and cavitation," *Int. J. Multiphase Flow* **113**, 208–230 (2019).
- ²⁹A. Chiapolino, P. Boivin, and R. Saurel, "A simple phase transition relaxation solver for liquid–vapor flows," *Int. J. Numer. Methods Fluids* **83**(7), 583–605 (2016).
- ³⁰A. Chiapolino, P. Boivin, and R. Saurel, "A simple and fast phase transition relaxation solver for compressible multicomponent two-phase flows," *Comput. Fluids* **150**, 31–45 (2017).
- ³¹J. Yu, J.-h. Liu, H.-k. Wang, J. Wang, L.-p. Zhang, and G.-z. Liu, "Numerical simulation of underwater explosion cavitation characteristics based on phase transition model in compressible multicomponent fluids," *Ocean Eng.* **240**, 109934 (2021).
- ³²J. Yu, J.-h. Liu, H.-k. Wang, J. Wang, Z.-t. Zhou, and H.-b. Mao, "Application of two-phase transition model in underwater explosion cavitation based on compressible multiphase flows," *AIP Adv.* **12**, 025209 (2022).
- ³³J. Zhang, "A simple and effective five-equation two-phase numerical model for liquid-vapor phase transition in cavitating flows," *Int. J. Multiphase Flow* **132**, 103417 (2021).